Synthesis and Reinforcement of Thermostable Polymers Using Renewable Resources

Nicole Segura Salas[1], Felipe Orozco Gutiérrez[3], Luis Daniel Mora Murillo[2], Yendry Corrales Ureña[3], Shakira Johnson[1], José Vega Baudrit[3] and Rodolfo Jesús González-Paz[3]*

[1]*Chemistry School, University of Costa Rica, San José, Costa Rica*
[2]*Chemical Engineering School, University of Costa Rica, San José, Costa Rica*
[3]*National Laboratory of Nanotechnology (LANOTEC), National Center of High Technology (CeNAT), San José, Costa Rica*

Received November 25, 2016; Accepted March 06, 2017

ABSTRACT: Vegetable oils are being used for the production of biodegradable polymers, opening new possibilities for the synthesis of greener materials that could compete in national markets with petroleum-based polymers. In this study, castor oil and a catalyst (cobalt[II] naphtenate as promotor and MEKP as initiator) from local stores and styrene in different ratios were used to produce thermostable polymers. The kinetics of the polymerization reaction was followed by infrared spectroscopy. A polymeric material was synthetized which presents good mechanical properties. Therefore, composites were produced using 1 wt% of microcellulose extracted from biomass waste as reinforcement or 1 wt% microsilica to improve the mechanical properties. The microfillers showed an improvement in the properties of composites by showing an increase in the Young's modulus. This easy production method can be suitable for small and medium companies who are trying to embrace responsible environmental consciousness.

KEYWORDS: Biobased polymers, silica microparticles, microcellulose, unsaturated polyester

1 INTRODUCTION

The growing interest in bioplastics due to environmental consciousness has led to the development of new research areas for new synthetic routes for the production of bioplastics based on renewable resources. Therefore, new legal requirements governing industry responsibility in terms of the environment are pushing for new and cleaner synthetic routes. These requirements have arisen due to the already known greenhouse emissions effect and pollution. The harmful environmental effects of plastic waste are associated with global warming and loss of natural species [1, 2]. The use of biobased materials is an alternative to reduce the quantity of waste due to their higher degradation rates [3, 4] and the possibility of being reused in applications as compostable organic materials in farms [4, 5].

In the last decade, sustainable sources such as vegetable oils have been widely investigated as substitutes for petroleum monomers because of their unsaturated bonds which can be copolymerized with other vinyl monomers and also their low price, inherent biodegradability and worldwide availability [6–9]. In general, biopolymers derived from oils do not match the mechanical properties to replace the petroleum-based polymers and fillers should be added to form composites [10–13]. Cellulose, for example, has been used as reinforcement fiber because of its low cost and high Young's modulus [14, 15]. Microsilica has also been used as filler to improve the material properties such as thermal stability and stiffness, Young's modulus and the fracture tenacity [16, 17]. In this research, castor oil and styrene (St) from local sources were used for the production of biopolymers. Polymer composites were prepared using cellulose and silica microparticles in order to improve the mechanical properties [18, 19].

2 EXPERIMENTAL SECTION

2.1 Materials

Maleic anhydride was supplied by Laboratorios Quimar and used without purification. Styrene monomer, cobalt(II) naphtenate 12% and MEKP 30% were purchased from Fibrocentro S.A. Castor oil was

*Corresponding author: rgonzalez@cenat.ac.cr

DOI: 10.7569/JRM.2017.634122

obtained from Malik S.A. Cellulose was extracted from pineapple peels supplied by Florida Products S.A. Castor oil was obtained from local stores with a hydroxyl value of 163.13 and an acid value of 0.25 and 87.26% of ricinoleic acid. Pirosil-PS200 (Valkimya Centroamerica) was used as microsilica particles, which have a size of 45 µm.

2.2 Synthesis of Maleinized Castor Oil (MaCO)

Castor oil (CO) was previously dried under reduced pressure for one hour. The esterification of CO with maleic anhydride was carried out under nitrogen atmosphere. Maleic anhydride was used in molar ratio of 2:1 (maleic anhydride to castor oil). The temperature was maintained using an oil bath at 120 °C and the reaction time was between 3–5 hours.

2.3 Acid Number Determination

A sample between 0.5–1 g was dissolved in 50 mL of toluene, then 5 mL of water was added and heated in a water bath at 50 °C during 30 minutes. Once the mixture was cooled down at room temperature, phenolphthalein was added. The acid number was determined by titration with 0.1 mol/L KOH in ethanol until the pink color lasted for 30 s. The acid number was calculated using Equation 1:

$$\text{Acid number} = \frac{56,1 * V * C}{M} \quad (1)$$

where V is the volume of KOH solution consumed, C is the concentration of the solution and M the sample weight.

2.4 Thermostable Biobased Polymer Preparation

For polymerization the styrene was bought from local stores and the maleate castor oil (MaCO) with variable ratios was measured in weight percentage. The polymerization was carried out under room conditions; concentration of additives was added by weight and reacted before the sample became viscous. MEKP was varied from 1–2 wt% and cobalt(II) naphtenate from 0.5–8 wt%. Then, the material was cured in an oven at 70 °C for two hours.

2.5 Microcrystalline Cellulose Preparation

Pineapple peels were placed in a solution of NaOH 20 wt%, at 70–90 °C for 1.5 hours. Next, they were rinsed and placed in NaOH 12% for 1 hour. The material was bleached with NaClO at 2.5 wt% for 2 hours at 60 °C. Afterwards, white cellulose was treated with HCl 17 wt% at 60 °C for 2 hours to obtain microcellulose.

2.6 Fourier Transform Infrared Spectroscopy (FTIR)

The FTIR spectra were recorded for the monitoring of reactions of esterification and polymerization. The measurements were made using a Nicolet 6700 Thermoscientific spectrometer in a range of 500–4000 cm^{-1} and a resolution of 4 cm^{-1}. This technique was used for monitoring the esterification reaction. The peak at 1730 cm^{-1} was used as an internal standard for monitoring the polymerization reaction [20].

2.7 Kinetic Measurements

Delahaye's [21] kinetic model for unsaturated polyester thermostable resins was used to study the polymerization reaction:

$$\alpha(t) = \alpha_{máx}(1 - e^{-\frac{t}{\tau}}) \quad (2)$$

where α is the functional group conversion through reaction, τ the time constant specific for each functional group and t the reaction time.

2.8 Dynamic Mechanical Analysis (DMA)

For DMA data, a DHR-3 rheometer was used for performing the mechanical analysis samples with dimensions of 60 × 14 × 1 (mm × mm × mm). The parameters used were shear rate of 1.6×10^{-5} s^{-1}.

2.9 Scanning Electron Microscopy (SEM)

The surface morphology of the microparticles, biopolymers and composite materials were investigated by using a scanning electron microscope (JEOL JSM-6390LV) at an accelerated voltage of 5–10 kV and a vacuum of $1E^{-4}$ Pa.

3 RESULTS AND DISCUSSION

3.1 Synthesis of MaCO

The maleinized castor oil (MaCO) used was a yellow-orange viscous material with an acid number of 90. The hydroxyl values and fatty acid percentage, specifically of ricinoleic acid, are very similar to those used by other authors to produce biopolymers based on this source [10–18]. Specifically, the hydroxyl value

is important because it equals the amount of double bonds in the structure, which are the sites for the crosslinking [11]. This indicates that a similar amount of crosslinking can be achieved with a local castor oil compared to other castor oils used by the authors mentioned above. The initial reaction was carried out using a molar ratio of 2:1 of maleic anhydride to castor oil; using this molar ratio the precipitation of maleic acid was avoided [10, 22]. The maleinization reaction was monitored by FTIR to understand the change in chemical bonds (Figure 1). The peak around ~1640 cm^{-1} corresponds to the -C=C- of maleic anhydride after reacting with hydroxyl content in castor oil and it was enhanced with the reaction time [23]. The absorption at ~1740 cm^{-1} corresponds to the carbonyl C=O moieties in castor oil and the peaks at 1850 and 1780 cm^{-1} correspond to the signals for cyclic maleic anhydride C=O symmetrical and asymmetrical vibrations, which seem to decrease in intensity at longer reaction times due to ring opening; indicating that the reaction is taking place [24]. Meanwhile, the broadening at 1740 cm^{-1} could be related to the increase of hydrogen bonding.

The versatile system could yield a variety of materials depending on the amount of additives and MaCO to styrene ratio in the synthesis. The reaction ratios used were 55:45 and 45:55 of MaCO to styrene, 3 wt% of commercial cobalt(II) naphtenate and 2 wt% of commercial MEKP. The ratios were chosen according to preliminary tests in which good mechanical properties were achieved. Both mixtures contained the same amount of additives, which led to a gelation time of approximately 20 min at room temperature. It was determined that 1 and 2 wt% of cobalt gave gelation times of 40 minutes and 25 minutes. Gelation times of 20 to 30 minutes were obtained with 3 wt% to 8 wt%. An intermediate value of 3 wt% of cobalt was chosen because at higher values than that the relation concentration/time did not increase between 8 wt% to 3 wt% as in the case of lower concentrations. This performance regarding the gelation time can be compared to other systems for unsaturated polyester resin reported in the literature [25].

The polymerization reaction was also monitored by FTIR spectroscopy, as shown in Figure 2.

Changes in carbon-carbon double bonds are observed in the range of 1640–1600 cm^{-1}. As polymerization reaction occurs, the peak signal of the double bond from the maleic anhydride moiety between 1640–1630 cm^{-1} decreases, becoming almost unnoticeable in Figure 2d and 2e [26]. Meanwhile, bands in 1600 cm^{-1}, 760 cm^{-1} and 1455 cm^{-1} arose from the polystyrene formation. Other peak bands at 980 cm^{-1} and 775 cm^{-1} described the consumption of the double bond in the MaCO chain and in the styrene monomer respectively; this will be followed quantitatively for the kinetic analysis in Figure 3. The curves obtained have the common shape for the curing of thermosetting resins [21, 27].

Using these kinetic measurements, time constants were obtained and compared with other reported data of similar systems. The time constant obtained of 25 min for styrene consumption is similar to the value reported by Delahaye *et al.* [18]. Meanwhile, for

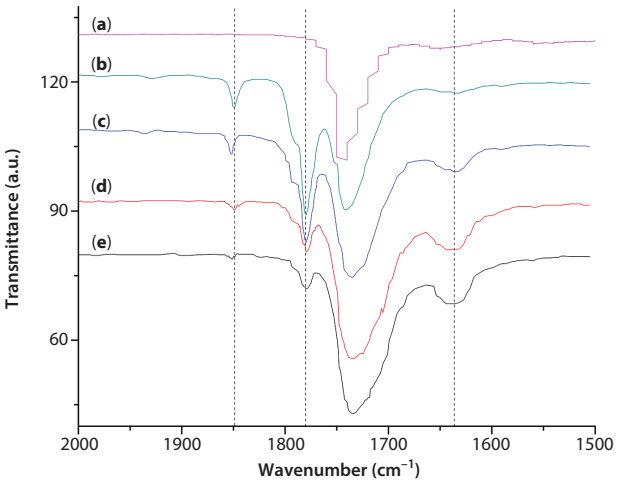

Figure 1 Maleinization reaction monitoring by FTIR spectroscopy: (**a**) Castor oil, (**b**) 15 min, (**c**) 40 min, (**d**) 100 min and (**e**) 140 min.

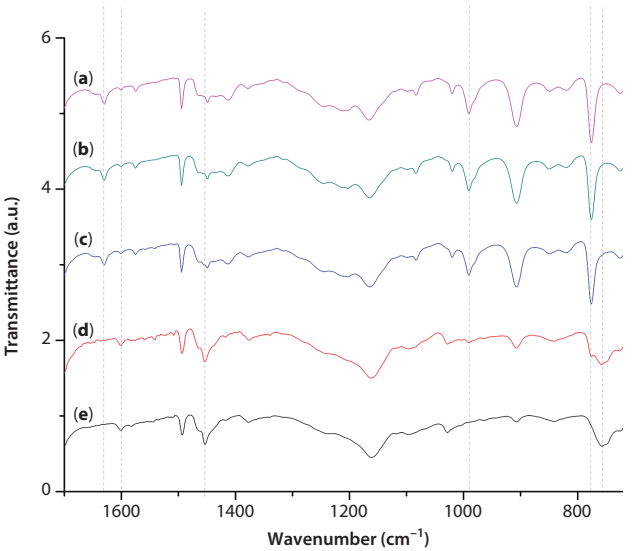

Figure 2 FTIR spectra comparison for the monitoring of the polymerization reaction of the system 55:45 MaCO:Styrene, 3 wt% cobalt(II) naphtenate and 2 wt% MEKP: (**a**) 0 min, (**b**) 10 min, (**c**) 40 min, (**d**) 15 min at 70°C and (**e**) 140 min at 70 °C .

 DOI: 10.7569/JRM.2017.634122

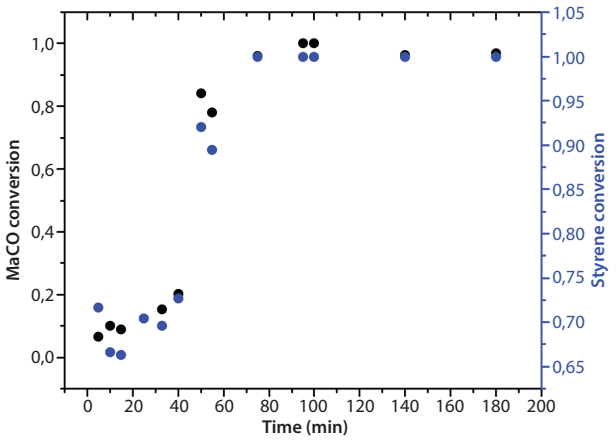

Figure 3 Rate of conversion of functional groups corresponding to • Styrene monomer (775 cm^{-1}) and • MaCO double bonds (980 cm^{-1}).

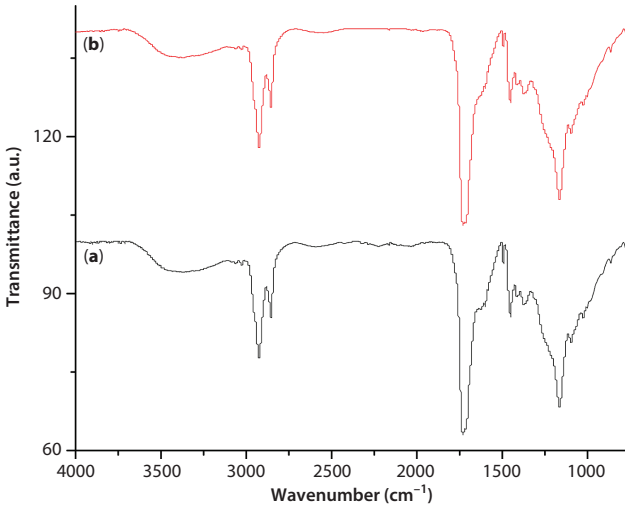

Figure 4 FTIR spectra of biobased polymer (**a**) 45:55 MaCO:St and (**b**) 55:45 MaCO:St.

the MaCO double bond it was 55 min, less than the one obtained by the same author. This result could be explained by an incomplete maleinization reaction. This is acceptable because the reaction time was shorter than that reported in the literature of 8 to 16 hours [10, 28, 29]. There is evidence of a faster conversion of styrene in the first minutes, relative to the consumption of the double bond in MaCO, which can be associated with evaporation of styrene or formation of polystyrene [30, 31]. The last hypothesis is more likely to happen because of the increase in the band at 1455 cm^{-1} product of the polystyrene formation. General characterization of the polymers is given in Figure 4.

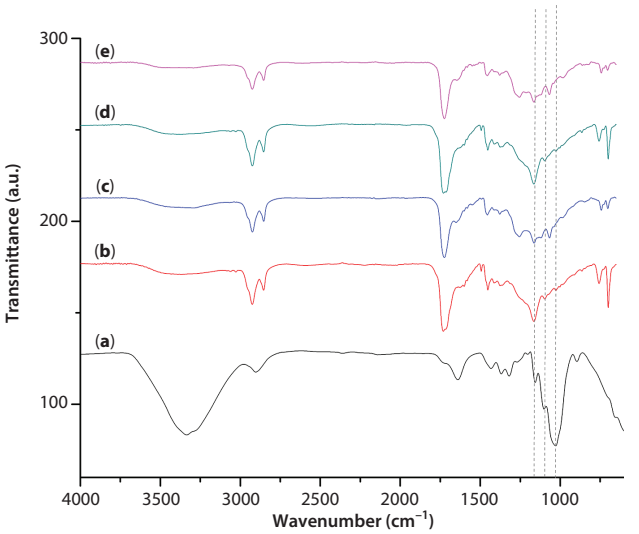

Figure 5 FTIR Spectra for (**a**) Microcellulose, (**b**) 45:55 MaCO:St, (**c**) 45:55 MaCO:St 1% microcellulose, (**d**) 55:45 MaCO:St and (**e**) 55:45 MaCO:St 1% microcellulose.

3.2 Characterization of Synthesized Biobased Polymer

Figure 4a and 4b shows the spectra of 45:55 MaCO:St and 55:45 MaCO:St and both exhibit a broad peak in the range of 2500–3000 cm^{-1} due to the presence of carboxylic acid groups. The peak at 1720 cm^{-1} corresponds to the vibration of the C=O group in the polymer network. The contributions of the asymmetric and symmetric vibration of the C-H are presented at 2926 and 2842 cm^{-1}. The peaks at 1444 and 1360 cm^{-1} are assigned to the symmetric bands of the alkyl groups $-CH_2$ and $-CH_3$, respectively. The peaks at 1242, 1165 and 1100 cm^{-1} are assigned to the -C-O- stretching [32].

The polymer without reinforcement has lower Young's modulus than polystyrene, as will be shown in the mechanical properties analysis section. For this reason, the addition of microcellulose or microsilica was used as a strategy for improving the mechanical properties.

Figure 5 shows the FTIR of the composite produced using microcellulose as a reinforcement. Figure 5a shows the spectra of the microcellulose with peaks assigned to the vibrational modes of specific functional groups [33–35]. The peaks at 1650 and 1730 cm^{-1} are associated with the carbonyl absorption and acyl group and uranic acid group of the hemicellulose. The appearance of the peak at 1274 cm^{-1} in Figure 5c and 5e is attributed to the split of C-O band because of hydrogen bonding of the microcellulose with the MaCO of the biobased polymer. This indicates that the microcellulose was physically blended with MaCO and they could have a good interaction [36].

Figure 6 shows the FTIR spectra of resin reinforced with microsilica. The pure silica typically exhibits three peaks centered at ~ 450 cm^{-1}, ~ 800 cm^{-1} and a broad peak at ~ 1100 cm^{-1}, as can be seen in Figure 6a. The absorption at ~ 450 cm^{-1} is assigned to the rocking motion of oxygen atoms bridging silicon atoms in siloxane bonds (Si-O-Si). The symmetric vibrations of silicon atoms in a siloxane bond occur at ~ 800 cm^{-1} and are called Si-O-Si. The largest peak observed in a silica spectrum is present at ~100 cm^{-1} and is dominated by the antisymmetric motion of silicon atoms in siloxane bonds [36–38].

It can be found that the peaks in the FTIR spectra of 45:55 MaCO:St 1 wt% microsilica and 55:45 MaCO:St 1 wt% microsilica exhibit a peak at 1274 cm^{-1}, due to the split of the original C-O band of the bioresin at 1168 cm^{-1}. This is attributed to the interference between the hydrogen bonding of the chains of the polymer and the silica, causing the number of hydrogen bonds to decrease between polymers chains. Therefore, the peak at ~1250 cm^{-1} was associated with the Si-O stretching. These changes in the spectra could be associated with the interaction of the silica with the polymer [39, 40].The silica could form a cation-π interaction between the silica metal atoms and the benzene ring of the polystyrene. There could be an interaction of the π-electrons of the aromatic ring and its specific Coulombic interaction with the silica atoms [41].

3.3 Mechanical Properties

The torsional behavior of the synthesized thermostable biobased polymers was studied and the results are shown in Figure 7. The diagram of stress-strain shows the influence of the styrene concentration in the polymer strength, where a smaller ratio of it in the resin gives more resistant polymers [42].

The morphology of the near surface polymer samples prepared using two composition ratios was examined by SEM. Figure 8a and 8b show smooth films; similar surface morphologies were observed. Figure 8c and 8d show the microsilica and mirocelullose particles. The silica particle presents roundish structures and particle sizes between 1–75 µm while microcellulose exhibits a preferential fibril structure with particle sizes between 5–200 µm.

Figure 9 shows the 45:55 and 55:45 surface structure of the biopolymers reinforced with 1 wt% of microsilica and microcellulose. Figure 9c and 9d shows single

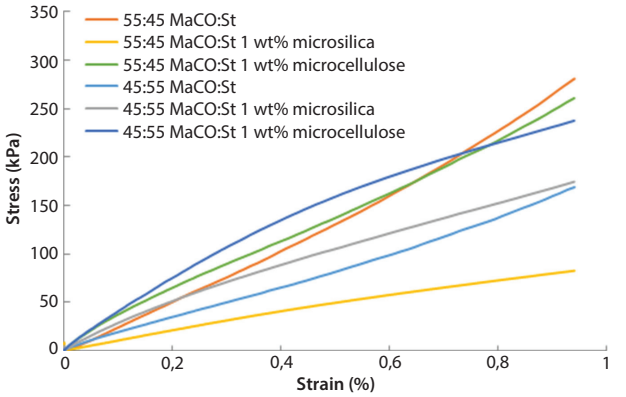

Figure 7 Stress-strain curves for biobased polymers of 45:55 and 55:45 MaCO:St ratios.

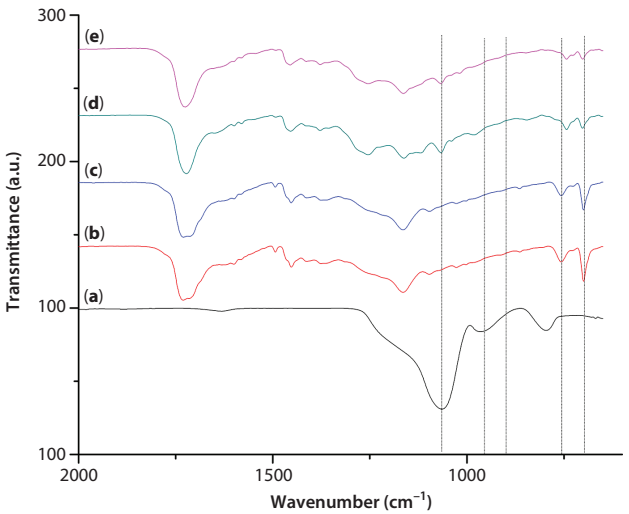

Figure 6 FTIR spectra for (**a**) Microsilica, (**b**) 45:55 MaCO:St, (**c**) 45:55 MaCO:St with 1% microsilica, (**d**) 55:45 MaCO:St and (**e**) 55:45 MaCO:St 1% microsilica.

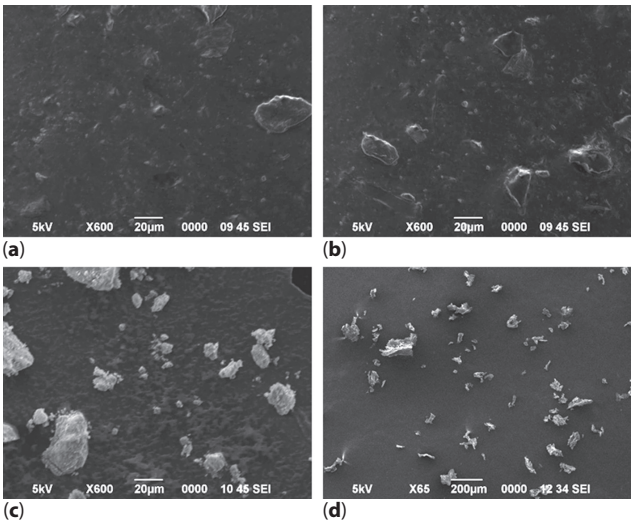

Figure 8 SEM micrographs of (**a**) MaCO:Styrene 45:55, (**b**) MaCO:St 45:55, (**c**) microsilica particles and (**d**) microcellulose.

particles with fibril-like morphology imaged near the surface, which is associated with microcellulose. Therefore, more electrodense (higher contrast with the carbon polymeric matrix) roundish particles were observed in Figure 9a and 9b, which are related to silica. A good dispersion of the microcellulose and the silica was obtained. The morphological effect of the microparticles using both compositions was similar. However, an increase in the surface roughness of the biopolymer containing microcellulose in comparison with the silica composites and the pristine polymers could be observed.

The composite material prepared with silica or microcellulose presented good dispersion of the microparticles. However, the microcellulose presented a higher increase in the mechanical properties, as can be seen in the stress-strain curves (see Figure 7). The dispersion is an important factor in improving the mechanical properties of a polymer with a filler, but also important is the interaction between them due to their chemical nature and the structure, size and crystallinity of the microparticles [43]. an increase in the mechanical properties is also an indication of possible good dispersion of the microparticles in the polymeric matrix [44].

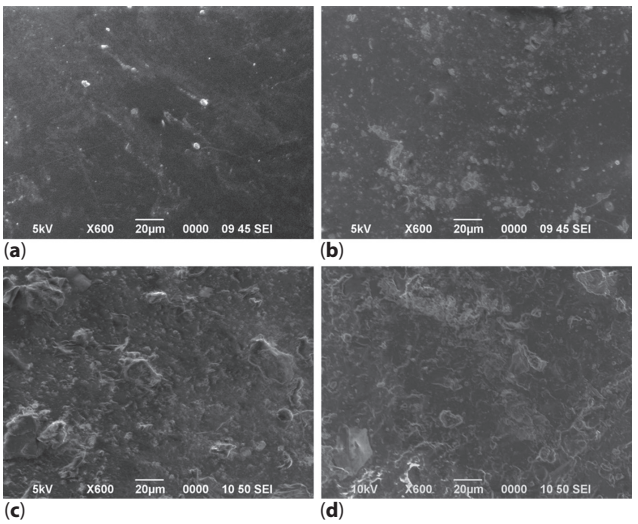

Figure 9 SEM micrographs of 1% MaCO:Styrene 45:55 (**a**) microsilica, (**b**) microcellulose and MaCO:Styrene 55:45, (**c**) microsilica and (**d**) microcellulose particle.

Microcellulose and microsilica gave an evident increase of the Young's modulus in the polymeric matrix prepared using 45:55 ratio and a reduction for that of 55:45 (see Table 1). This could be related to the nonhomogeneous dispersion in the media due to the higher viscosity of the resin; when the styrene ratio decreases in the mixture its viscosity increases [45]. Nonetheless, the effect of the reinforcement can be seen in the composites, showing a better performance when a higher amount of St is present, this is because a more homogenous mix was achieved. Thus, promotion of the polymer-microparticle interaction increases the glass transition of the polymer matrix (see Table 1).

Thermal stability of resins with different MaCO:St compositions was determined by thermogravimetric analysis (TGA), as shown in Figure 10, including samples with and without reinforcement materials. Thermal stability is mostly related to degradation of C=C bonds (styrene chains) and ester and acid bonds in MaCO chains. The TGA curves show differences in the behavior between MaCO-St matrix and silica or cellulose reinforcement by analyzing changes in the $T_{10\%}$ (temperature at which 10% of sample weight has been lost). Table 1 shows that the silica reinforcement implies a lower degradation temperature of the resins because the presence of silica interferes with the polymer chain-chain interactions, as shown by FTIR in Figure 6. Cellulose reinforcement implies a higher $T_{10\%}$ than those samples with silica reinforcement because of the presence of many O-H groups that promote H bonding between the polymer chains and microparticles, which improves the stability of chain bonds. In general, there is only one mass loss stage of decomposition at ~ 275 °C to ~ 400 °C. There is a little drop at 200 °C that can be associated with the evaporation

Table 1 Mechanical and thermal properties of biobased thermostable polymers.

Sample	E_{tor} [a](MPa)	T_g [a](°C)	$T_{10\%}$ [b](°C)	T_g [c](°C)
45:55 MaCO:St	1,65	51	264	18
55:45 MaCO:St	2,68	54	267	19
45:55 MaCO:St with 1 wt% silica	2.02	54	259	29
55:45 MaCO:St with 1 wt% silica	0,96	32	242	10
45:55 MaCO:St with 1 wt% cellulose	2,99	58	268	36
55:45 MaCO:St with 1 wt% cellulose	2,71	55	274	37

*Values obtained by [a] Rheometer-DMTA, [b] TGA and [c] DSC

of unreacted monomers and other volatile substances incorporated into the resin matrix [46–49]. Therefore, Table 1 shows the glass transition temperatures of 45:55 MaCO:St and 55:45 MaCO:St of resins measured by using DSC, where a difference of 3 °C is appreciated; the higher content of MaCO increases the crosslink between polymer chains and mobility is more restricted, so more energy is needed to move the polymer chains [42]. The polymer network is affected by crosslink density [50], so higher T_g means that the matrix of the polymer is crosslinked better than materials with lower T_g. Intermolecular forces also affect the changes of glass transition temperatures because high intermolecular forces in the matrix cause polymeric network to have less mobility, so it needs more temperature to flow [51].

Figure 11 shows the storage modulus (G′) curves for the biobased thermostable polymers. These curves are obtained by DMTA testing, a method that measures the response of a given material to a cyclic deformation as a function of temperature. MaCO:St resins show differences in the G′ curve, indicating the influence of the composition on the elastic properties of the matrix. The variation of storage modulus (G′) of composites in Figure 12 shows that the initial G′ values were higher for the resins without reinforcement. The higher values of G′ for resins without reinforcement are related to the capacity of the polymer network to absorb the energy that is applied during the test. There is a unique behavior of the G′ curve for 55:45 MaCO:St because it started decreasing, then there was a little increase in storage modulus in the temperature from 80 °C. This increase in storage modulus could exist due to the condensation reaction occurring between the MaCO molecules in close proximity with each other in the formed polymer network [52].

Figure 12 shows dependence of the tan δ with increasing the temperature of the biobased resins. All the tan δ curves demonstrated similar behaviors and glass transition temperature (T_g) can also be measured by this method; this data is listed in Table 1. The T_g is determined by the peak temperature of tan δ.

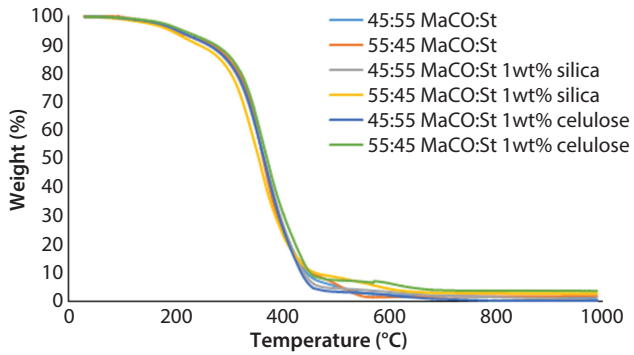

Figure 10 Thermogravimetric analysis of biobased polymers of 45:55 and 55:45 MaCO:St ratios.

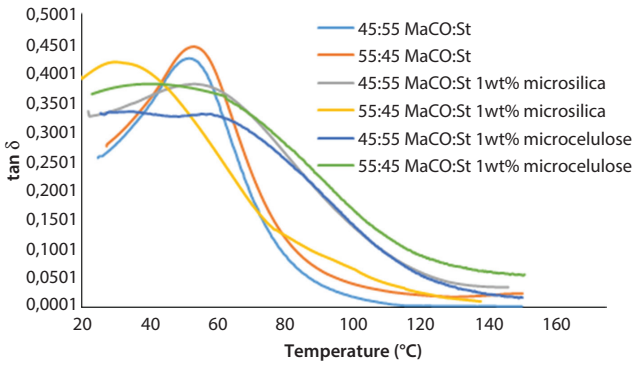

Figure 12 Biobased polymers of 45:55 and 55:45 MaCO:St ratios curves for tan δ behavior with temperature increase.

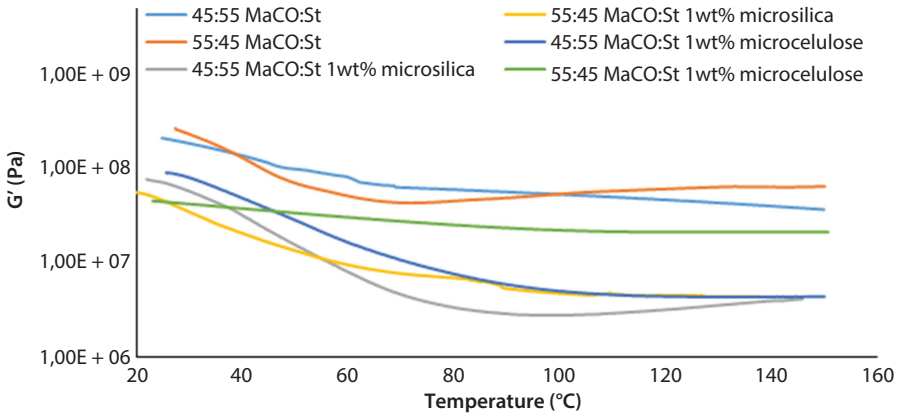

Figure 11 Storage modulus curves for bioresins of 45:55 and 55:45 MaCO:St ratios.

Microcellulose can help in the orientation of the chains of the crosslinked polymer along the matrix axis, improving the mechanical properties of the material [53]. According to Table 1, composites with 1 wt% of microcellulose have the higher T_g, and due to interactions that appear when the cellulose is added, more H bonds and crosslinked networks can be achieved, adding cellulose content. On the other hand, 55:45 MaCO:St with 1 wt% of microsilica reaches a lower T_g; in this case it is possible that van der Waals forces are affected by the microparticles and chains can move more, so microsilica has a plasticizer effect [51, 54]. According to the above results, we can conclude that 45:55 MaCO:St with 1 wt% of microcellulose system has the better result, showing a higher performance as composite material.

4 CONCLUSIONS

Using a Costa Rican castor oil, maleinization was successfully achieved for the production of a competent thermostable polymer. The system was optimized at room temperature with a gel time of 20 min with 3 wt% cobalt(II) naphtenate and 2 wt% MEKP. The kinetics of the polymerization reaction, followed by FTIR, was close to those reported by other authors and depends on the time of maleinization as well as the amount of styrene. The polymer synthesized is promising as a potential material for industrial applications in terms of low-cost materials and cheap processing. Generally, the use of reinforcement in the thermostable polymers gave harder final resins than those that do not have microcellulose or microsilica. Reinforcement with nanomaterials is being tested for a resin with mechanical properties as well as commercial ones.

ACKNOWLEDGMENT

We thank Govan Projects S.A. for supplying the reagents and material during the course of this project.

REFERENCES

1. C.M. Rochman, M.A. Browne, B.S. Halpern, B.T. Hentschel, E. Hoh, H.K. Karapanagioti, L.M. Rios-Mendoza, H. Takada, S. Teh, and R.C. Thompson, Policy: Classify plastic waste as hazardous. *Nature* **494**, 169–171 (2013).
2. E.L. Teuten, J.M. Saquing, D.R.U. Knappe, M.A. Barlaz, S. Jonsson, A. Björn, S.J. Rowland, R.C. Thompson, T.S.Galloway,R.Yamashita,D.Ochi,Y.Watanuki,C.Moore, P.H. Viet, T.S. Tana, M. Prudente, R. Boonyatumanond, M.P. Zakaria, K. Akkhavong, Y. Ogata, H. Hirai, S. Iwasa, K. Mizukawa, Y. Hagino, A. Imamura, M. Saha, H. Takada, Transport and release of chemicals from plastics to the environment and to wildlife. *Philos. Trans. R. Soc. Lond. B. Biol. Sci.* **364**, 2027–2045 (2009).
3. G. Davis and J.H. Song, Biodegradable packaging based on raw materials from crops and their impact on waste management. *Ind. Crops Prod.* **23**, 147–161 (2006).
4. J.H. Song, R.J. Murphy, R. Narayan, and G.B.H. Davies, Biodegradable and compostable alternatives to conventional plastics. *Philos. Trans. R. Soc. B Biol. Sci.* **364**, 2127–2139 (2009).
5. J. Lörcks, Properties and applications of compostable starch-based plastic material. *Polym. Degrad. Stab.* **59**, 245–249 (1998).
6. J. Deng, B. Yang, C. Chen, and J. Liang, Renewable eugenol-based polymeric oil-absorbent microspheres: Preparation and oil absorption ability. *ACS Sustain. Chem. Eng.* **3**, 599–605 (2015).
7. G. Lligadas, J.C. Ronda, M. Galià, and V. Cádiz, Renewable polymeric materials from vegetable oils: A perspective. *Mater. Today* **16**, 337–343 (2013).
8. L.M. de Espinosa and M.A.R. Meier, Plant oils: The perfect renewable resource for polymer science?! *Eur. Polym. J.* **47**, 837–852 (2011).
9. F.S. Güner, Y. Yağci, and A.T. Erciyes, Polymers from triglyceride oils. *Prog. Polym. Sci.* **31**, 633–670 (2006).
10. M.A. Saied, S.H. Mansour, M. Eweis, M.Z. El-Sabee, A.L.G. Saad, and K.N. Abdel Nour, Some biophysical properties of castor oil esterified with some acid anhydrides. *Eur. J. Lipid Sci. Technol.* **110**, 926–934 (2008).
11. G.M. Yenwo, J.A. Manson, J. Pulido, L.H. Sperling, A. Conde, and N. Devia, Castor-oil-based interpenetrating polymer networks: Synthesis and characterization. *J. Appl. Polym. Sci.* **21**, 1531–1541 (1977).
12. Y. Xia and R.C. Larock, Vegetable oil-based polymeric materials: Synthesis, properties, and applications. *Green Chem.* **12**, 1893–1909 (2010).
13. P. Ferreira, R. Pereira, J.F.J. Coelho, A.F.M. Silva, and M.H. Gil, Modification of the biopolymer castor oil with free isocyanate groups to be applied as bioadhesive. *Int. J. Biol. Macromol.* **40**, 144–152 (2007).
14. W. Gacitua, A. Ballerini, and J. Zhang, Polymer nanocomposites: Synthetic and natural fillers a review. *Maderas. Cienc. y Tecnol.* **7**, 159–178 (2005).
15. M.K.M. Haafiz, A. Hassan, Z. Zakaria, I.M. Inuwa, M.S. Islam, and M. Jawaid, Properties of polylactic acid composites reinforced with oil palm biomass microcrystalline cellulose. *Carbohydr. Polym.* **98**, 139–145 (2013).
16. T. Mahrholz, J. Stängle, and M. Sinapius, Quantitation of the reinforcement effect of silica nanoparticles in epoxy resins used in liquid composite moulding processes. *Compos. Part A* **40**, 235–243 (2009).
17. P. Rosso, L. Ye, K. Friedrich, and S. Sprenger, A toughened epoxy resin by silica nanoparticle reinforcement. *J. Appl. Polym. Sci.* **100**, 1849–1855 (2006).
18. A.K. Mohanty, M. Misra, and G. Hinrichsen, Biofibres, biodegradable polymers and biocomposites: An overview. *Macromol. Mater. Eng.* **276–277**, 1–24 (2000).

19. M. Wollerdorfer and H. Bader, Influence of natural fibres on the mechanical properties of biodegradable polymers. *Ind. Crops Prod.* **8**, 105–112 (1998).
20. M. Gutekin, U. Beker, F.S. Güner, A.T. Erciyes, and Y. Yagci, Styrenation of castor oil and linseed oil by macromer method Styrenation of castor oil and linseed oil by macromer method. *Macromol. Mater. Eng.* **2054**, 15–20 (2015).
21. N. Delahaye, S. Marais, J.M. Saiter, and M. Metayer, Characterization of unsaturated polyester resin cured with styrene. *J. Appl. Polym. Sci.* **67**, 695–703 (1998).
22. H.J. Wang, M.Z. Rong, M.Q. Zhang, J. Hu, H.W. Chen, and T. Czigány, Biodegradable foam plastics based on castor oil. *Biomacromolecules* **9**, 615–623 (2008).
23. S. Kumari, D. Nigam, D. Agarwal, and I. Nigam, Synthesis and characterization of alkali-modified styrene-maleic anhydride copolymer for dispersion of TiO_2. *J. Appl. Polym. Sci.* **103**, 3194–3205 (2007).
24. Y. Zhou, X. Yang, and D. Jia, Cure behavior of unsaturated polyester/modified montmorillonite nanocomposites. *Polym. Int.* **56**, 267–274 (2007).
25. R.S. Rajput, D.C. Rupainwar, R.K. Singh, and A. Singh, Study on characterization and degree of esterification of styrene maleic anhydride by some medicines. *Indian J. Chem. B* **48**, 1597–1600 (2009).
26. G.S. Learmonth and G. Pritchard, Cure of polyester resins—determination by infra-red spectroscopy. *Polym. Int.* **1**, 88–93 (1969).
27. H. Warth, R. Mülhaupt, B. Hoffmann, and S. Lawson, Polyester networks based upon epoxidized and maleinated natural oils. *Die Angew. Makromol. Chemie* **249**, 79–92 (1997).
28. T. Eren, S.H. Küsefoglu, and R. Wool, Polymerization of maleic anhydride-modified plant oils with polyols. *J. Appl. Polym. Sci.* **90**, 197–202 (2003).
29. Y.-J. Huang, T.-J. Lu, and W. Hwu, Curing of unsaturated polyester resins—effects of pressure. *Polym. Eng. Sci.* **33**, 1–17 (1993).
30. K.W. Lem and C.D. Han, Chemorheology of thermosetting resins. II. Effect of particulates on the chemorheology and curing kinetics of unsaturated polyester resin. *J. Appl. Polym. Sci.* **28**, 3185–3206 (1983).
31. B.P. Vibhute, R.R. Khotpal, V.Y. Karadbhajane, and A.S. Kulkarni, Preparation of maleinized castor oil (MCO) by conventional method and its application in the formulation of liquid detergent. *Int. J. ChemTech Res.* **5**, 1886–1896 (2013).
32. I.K.I. Al-Khateeb, S.M. Hussin, and Y.M. Al-Obaidi, Extraction of cellulose nano crystalline from cotton by ultrasonic and its morphological and structural characterization. *Int. J. Mater. Chem. Phys.* **1**, 99–109 (2015).
33. J. George and S.N. Sabapathi, Cellulose nanocrystals: Synthesis, functional properties, and applications. *Nanotechnol. Sci. Appl.* **8**, 45–54 (2015).
34. A. Kumar, Y.S. Negi, V. Choudhary, and N.K. Bhardwaj, Characterization of cellulose nanocrystals produced by acid-hydrolysis from sugarcane bagasse as agro-waste. *J. Mater. Phys. Chem.* **2**, 1–8 (2014).
35. S. Huan, L. Bai, G. Liu, W. Cheng, and G. Han, Electrospun nanofibrous composites of polystyrene and cellulose nanocrystals: manufacture and characterization. *RSC Adv.* **5**, 50756–50766 (2015).
36. G.E.A. Swann and S.V. Patwardhan, Application of fourier transform infrared spectroscopy (FTIR) for assessing biogenic silica sample purity in geochemical analyses and palaeoenvironmental research. *Clim. Past* **7**, 65–74 (2011).
37. Y. Li, B. Han, S. Wen, Y. Lu, H. Yang, L. Zhang, and L. Liu, Effect of the temperature on surface modification of silica and properties of modified silica filled rubber composites. *Compos. Part A Appl. Sci. Manuf.* **62**, 52–59 (2014).
38. F. Ghorbani, H. Younesi, Z. Mehraban, M.S. Çelik, A.A. Ghoreyshi, and M. Anbia, Preparation and characterization of highly pure silica from sedge as agricultural waste and its utilization in the synthesis of mesoporous silica MCM-41. *J. Taiwan Inst. Chem. Eng.* **44**, 821–828 (2013).
39. A.P. Wight and M.E. Davis, Design and preparation of organic-inorganic hybrid catalysts. *Chem. Rev.* **102**, 3589–3614 (2002).
40. J. Choi, J. Harcup, A.F. Yee, Q. Zhu, and R.M. Laine, Organic/inorganic hybrid composites from cubic silsesquioxanes. *J. Am. Chem. Soc.* **123**, 11420–11430 (2001).
41. B. Coasne, and J.T. Fourkas, Structure and dynamics of benzene confined in silica nanopores. *J. Phys. Chem. C* **115**, 15471–15479 (2011).
42. E.M.S. Sanchez, C.A.C. Zavaglia, and M.I. Felisberti, Unsaturated polyester resins: Influence of the styrene concentration on the miscibility and mechanical properties. *Polymer (Guildf.)* **41**, 765–769 (2000).
43. S. Wacharawichanant, A. Sangkhaphan, N. Sa-Nguanwong, V. Khamnonwat, S. Thongyai, and P. Praserthdam, Effects of particle type on thermal and mechanical properties of polyoxymethylene nanocomposites. *J. Appl. Polym. Sci.* **123**, 3217–3224 (2012).
44. M. Conradi, Nanosilica-reinforced polymer composites. *Mater. Tehnol.* **47**, 285–293 (2013).
45. L.A. Wall, S. Straus, J.H. Flynn, D. McIntyre, and R. Simha, The thermal degradation mechanism of polystyrene. *J. Phys. Chem.* **70**, 53–62 (1966).
46. W.R. Zeng, W.K. Chow, and B. Yao, Chemical kinetics and mechanism of polystyrene thermal decomposition. *Asia-Oceania Symp. Fire Sci. Technol. Fire Chem.* (2007).
47. M. Yang and Y. Shibasaki, Mechanisms of thermal degradation of polystyrene, polymethacrylonitrile and their copolymers on flash pyrolysis. *J. Therm. Anal.* **49**, 71–77 (1997).
48. M. Liehr, Kinetics of high-temperature thermal decomposition of SiO_2 on Si(100). *J. Vac. Sci. Technol. A Vacuum, Surfaces, Film.* **5**, 1559 (1987).
49. R. Tromp, G.W. Rubloff, P. Balk, and F.K. Legoues, High-temperature $Si0_2$ decomposition at the SiOa Si interface. *Phys. Rev. Lett.* **55**, 2332–2337 (1985).
50. I.-Y. Jeon and J.-B. Baek, Nanocomposites derived from polymers and inorganic nanoparticles. *Materials (Basel)* **3**, 3654–3674 (2010).
51. J. Dai, S. Ma, Y. Wu, L. Han, L. Zhang, J. Zhu, and X. Liu, Polyesters derived from itaconic acid for the

properties and bio-based content enhancement of soybean oil-based thermosets. *Green Chem.* **17**, 2383–2392 (2015).
52. E. Mistri, S. Routh, D. Ray, S. Sahoo, and M. Misra, Green composites from maleated castor oil and jute fibres. *Ind. Crops Prod.* **34**, 900–906 (2011).
53. C. Miao and W.Y. Hamad, Cellulose reinforced polymer composites and nanocomposites: A critical review. *Cellulose* **20**, 2221–2262 (2013).
54. C.-H. Lee and J.-J. Park, The properties of DSC and DMA for epoxy nano- and micro-mixture composites. *Trans. Electr. Electron. Mater.* **11**, 69–72 (2010).